# Long-term NO$_x$ measurements in the remote marine tropical troposphere

Simone T. Andersen[1*], Lucy J. Carpenter[1], Beth S. Nelson[1], Luis Neves[2], Katie A. Read[1,3], Chris Reed[4], Martyn Ward[1], Matthew J. Rowlinson[1,3], James D. Lee[1,3]

[1]Wolfson Atmospheric Chemistry Laboratories (WACL), Department of Chemistry, University of York, Heslington, York, YO10 5DD, UK.

[2] Instituto Nacional de Meteorologia e Geofísica, São Vicente (INMG), Mindelo, Cabo Verde.

[3]National Centre for Atmospheric Science (NCAS), University of York, Heslington, York, YO10 5DD, UK.

[4]FAAM Airborne Laboratory, Building 146, Cranfield University, Cranfield, MK43 0AL, UK.
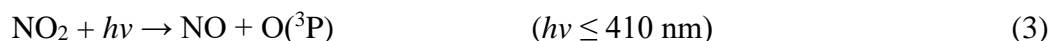
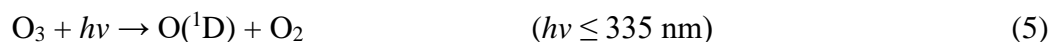[*]Corresponding author: sta516@york.ac.uk

# Abstract

Atmospheric nitrogen oxides ($NO + NO_2 = NO_x$) have been measured at the Cape Verde Atmospheric Observatory (CVAO) in the tropical Atlantic (16° 51' N, 24° 52' W) since October 2006. These measurements represent a unique time series of $NO_x$ in the background remote troposphere. Nitrogen dioxide ($NO_2$) is measured via photolytic conversion to nitric oxide (NO) by ultra violet light emitting diode arrays followed by chemiluminescence detection. Since the measurements began, a "blue light converter" (BLC) has been used for $NO_2$ photolysis, with a maximum spectral output of 395 nm from 2006-2015 and of 385 nm from 2015. The original BLC used was constructed with a Teflon-like material and appeared to cause an overestimation of $NO_2$ when illuminated. To avoid such interferences, a new additional photolytic converter (PLC) with a quartz photolysis cell (maximum spectral output also 385 nm) was implemented in March 2017. Once corrections are made for the $NO_2$ artefact from the original BLC, the two $NO_2$ converters are shown to give comparable $NO_2$ mixing ratios (~~B~~PLC = 0.99~~2~~ × P~~B~~LC + 0.7 ppt~~, R² = 0.92~~, linear least squares regression), giving confidence in the quantitative measurement of $NO_x$ at very low levels. Data analysis methods for the $NO_x$ measurements made at CVAO have been developed and applied to the entire time series to produce an internally consistent and high quality long-term data set. NO has a clear diurnal pattern with a maximum mixing ratio of 2-10 ~~pptV~~ppt during the day depending on the season and ~0 ~~pptV~~ppt during the night. $NO_2$ shows a fairly flat diurnal signal, although a small increase in daytime $NO_x$ is evident in some months. Monthly average mixing ratios of $NO_2$ vary between 5 and 30 ~~pptV~~ppt depending on the season. Clear seasonal trends in NO and $NO_2$ levels can be observed with a maximum in autumn/winter and a minimum in spring/summer.

# 1 Introduction

Atmospheric nitrogen oxides play a key role in tropospheric chemistry. $NO_x$ helps to control the abundance of the two most important oxidants in the atmosphere, ozone ($O_3$) and the hydroxyl radical (OH). The presence of NO is usually the key limiting factor in the production of tropospheric $O_3$, which occurs via oxidation of NO to $NO_2$ by peroxy radicals ($RO_2$, $HO_2$) as described in reactions (1-2), followed by photolysis of $NO_2$ and rapid conversion of the resulting $O(^3P)$ to $O_3$:

$$RO_2 + NO \rightarrow RO + NO_2 \tag{1}$$

$$HO_2 + NO \rightarrow OH + NO_2 \tag{2}$$

$$NO_2 + hv \rightarrow NO + O(^3P) \qquad (hv \leq 410 \text{ nm}) \tag{3}$$

$$O(^3P) + O_2 + M \rightarrow O_3 + M \tag{4}$$

Reaction (2) also offers a route to the OH radical, above its primary production via $O_3$ photolysis (reactions (5) and (6)). If the $NO_x$ mixing ratio is sufficiently low, then peroxy radicals react with themselves instead of NO, and $O_3$ depleting reactions (reactions (5) to (8)) dominate over $O_3$ production (Atkinson, 2000).

$$O_3 + hv \rightarrow O(^1D) + O_2 \qquad (hv \leq 335 \text{ nm}) \tag{5}$$

$$O(^1D) + H_2O \rightarrow 2 \text{ OH} \tag{6}$$

$$OH + O_3 \rightarrow HO_2 + O_2 \tag{7}$$

$$HO_2 + O_3 \rightarrow OH + 2 O_2 \tag{8}$$

It is assumed that, under tropospheric conditions at the low mole fractions discussed, NO and $NO_2$ behave as ideal gases and therefore mole fraction (picomole/mole, the appropriate SI unit) is equivalent to volumetric mixing ratio, represented by part per trillion (ppt). $NO_x$ mixing ratios below 10-30 ~~pptV~~ppt are generally sufficiently low for net tropospheric $O_3$ depletion (Atkinson, 2000; Jaeglé et al., 1998; Logan, 1985). These conditions have previously been reported to apply most of the year in the remote Atlantic Ocean (Lee et al., 2009). The mixing ratio of $NO_x$ in the atmosphere varies from a few ~~pptV~~ppt in remote areas (Lee et al., 2009; Monks et al., 1998; Reed et al., 2017) to >100 ppb~~V~~ in polluted areas (Berkes et al., 2018; Carslaw, 2005; Mazzeo et al., 2005; Pandey et al., 2008). It is therefore important to have

67 representative $NO_x$ measurements in different regions of the world to be able to understand the
68 chemistry occurring throughout the troposphere.

69 Long-term remote atmospheric $NO_x$ measurements are rare due to the difficulty measuring
70 very low (~~pptV~~ppt) mixing ratios. Many different methods of measuring $NO_x$ are available,
71 however, very few have the limit of detection (LOD) and sensitivity needed to measure $NO_x$
72 in remote regions. The most widely used method is NO chemiluminescence, where NO in the
73 presence of excess ozone is oxidized into excited state $NO_2$, which emits photons that can be
74 detected (Fontijn et al., 1970). $NO_2$ is generally converted into NO either catalytically by a
75 heated molybdenum converter or photolytically, followed by NO chemiluminescence (Kley
76 and McFarland, 1980). The molybdenum converter has historically been preferred due to its
77 high conversion efficiency of at least 95%, but it also converts other <u>reactive nitrogen species</u>
78 <u>(NOz) such as peroxyacetyl nitrate (PAN), peroxymethacryloyl nitrate (MPAN) and other acyl</u>
79 <u>peroxy nitrates (APN)</u>~~reactive nitrogen species (NO_z) such as peroxyacetyl nitrate (PAN),~~
80 ~~peroxymethacryloyl nitrate (MPAN), acyl peroxy nitrates (APN)~~, $HNO_3$, p-$HNO_3$, <u>$HO_2NO_2$,</u>
81 and HONO, potentially giving an overestimation of $NO_2$ (Dunlea et al., 2007; Grosjean and
82 Harrison, 1985; Winer et al., 1974). Two separate studies have shown that photolytic converters
83 (PLC) with a wavelength of 385-395 nm have the smallest spectral overlap with interfering
84 compounds (Pollack et al., 2010; Reed et al., 2016). Reed et al., (2016) showed that in some
85 configurations the PLC can heat up the sampled air making it possible for reactive nitrogen
86 compounds such as ~~peroxyacetyl nitrate (~~PAN~~)~~ to decompose thermally and cause an
87 overestimation of $NO_2$. This, however, causes only a negligible interference in warm regions
88 such as Cabo Verde where PAN levels are extremely low (Reed et al., 2016).

89 In this study we describe a $NO_2$ converter, similar to that presented by Pollack et al. (2010),
90 which has been implemented on an instrument to measure $NO_x$ at the CVAO. The data analysis
91 procedure is explained in detail and the first two years of results with the new converter are
92 presented and compared to the data obtained using a different converter.
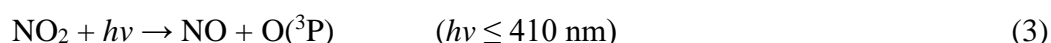
93

## 2 Experimental

### 2.1 Location

96 The Cape Verde Atmospheric Observatory (CVAO; 16° 51' N, 24° 52' W) is located on
97 the north eastern coast of São Vicente, Cabo Verde. The air masses arriving at the CVAO

98   predominately come from the northeast (>95% of all wind direction measurements, see Figure
99   1) and have travelled over the Atlantic Ocean for multiple days since their last exposure to
100  anthropogenic emissions, with the potential exception of ship emissions (Carpenter et al., 2010;
101  Read et al., 2008). The UK Meteorological Office NAME dispersion model (Ryall et al., 2001)
102  has previously been used to investigate the origin of the air masses arriving at the CVAO,
103  which have been shown to be very diverse; North America, the Atlantic, Europe, Arctic, and
104  African regions (Lee et al., 2009). During the spring and summer, the air masses predominantly
105  originate from the Atlantic making it possible to investigate long-term remote marine
106  tropospheric background measurements. During the winter, the CVAO receives air mainly
107  from the Sahara, resulting in very high wintertime dust loadings (Chiapello et al., 1995; Fomba
108  et al., 2014; Rijkenberg et al., 2008). The time zone of Cabo Verde is ~~always~~ UTC-1. A full
109  description of the CVAO site and associated measurements is given in Carpenter et al. (2010).

110

## 2.2  Measurement Technique

112     $NO_x$ has been measured at the CVAO since 2006 using a $NO_x$ chemiluminescence
113  instrument manufactured by Air Quality Design Inc. (AQD), USA.  The chemiluminescence
114  technique involves the oxidation of NO by excess $O_3$ to excited $NO_2$ (Reaction 9) (Clough and
115  Thrush, 1967; Clyne et al., 1964; Fontijn et al., 1970). The excited $NO_2$ molecules can be
116  deactivated by emitting photons (Reaction 10) or by being quenched by other molecules
117  (Reaction ~~10 and~~ 11) such as $N_2$, $O_2$, and in particular $H_2O$. The emitted photons are detected
118  by a photomultiplier tube detector (PMT), which gives a signal linearly proportional to the
119  mixing ratio of NO sampled. The measurement of $NO_x$ and $NO_2$ requires photolytic conversion
120  of $NO_2$ to NO (Reaction 3) followed by NO chemiluminescence detection (Kley and
121  McFarland, 1980).

122     $NO + O_3 \rightarrow NO_2^* + O_2$                                          (9)

123     $NO_2^* \rightarrow NO_2 + hv$            ($hv > 600$ nm)                     (10)

124     $NO_2^* + M \rightarrow NO_2$                                              (11)

125     $NO_2 + hv \rightarrow NO + O(^3P)$         ($hv \leq 410$ nm)                  (3)

126  Further details of the technique are documented in (Carpenter et al., 2010; Drummond et al.,
127  1985; Fontijn et al., 1970; Lee et al., 2009; Peterson and Honrath, 1999; Reed et al., 2017; Val
128  Martin et al., 2006).

## 2.3  Instrument Set-up

Ambient air is sampled from a downward facing inlet placed into the prevailing wind with a fitted hood 10 m above the ground. A centrifugal pump at a flow rate of ~750 litres per minute pulls the air into a 40 mm glass manifold resulting in a linear sample flow of 10 m s$^{-1}$, giving a residence time to the inlet of the $NO_x$ instrument of 2.3 s. To reduce the humidity and aerosol concentration in the sampled air, dead-end traps are placed at the lowest point of the manifold inside and outside the laboratory. A Nafion dryer (PD-50T-12-MKR, Permapure) is used to additionally dry the sampled air, using a constant sheath flow of zero air (PAG 003, Eco Physics AG) that has been filtered through a Sofnofil (Molecular Products) and activated charcoal (Sigma Aldrich) trap (dewpoint -15°C). The air is sampled perpendicular to the manifold through a 47mm PTFE (polytetrafluoroethylene) filter with a pore size of 1.2 μm.

A schematic diagram of the instrument is shown in Figure 2.  Sampled air is passed through two different photolytic $NO_2$ converters, which are placed in series.  The first is a commercial unit known as a BLC (Blue Light Converter) supplied by Air Quality Design, as described in (Buhr, 2007). An ultra violet light emitting diode (UV-LED, 3 W, LED Engin, Inc.) array is placed in each end of a reaction chamber made of Teflon-like barium doped material (BLC, λ = 385 nm, volume = 16 cm$^3$). The entire block surrounding the reaction chamber is irradiated, giving the highest possible conversion efficiency of $NO_2$. Each array is cooled by a heat sink to maintain an approximately constant temperature inside of the converter when the diode arrays turn on. The second converter consists of two diodes (Hamamatsu Lightningcure L11921-500, λ = 385 nm) and a photolysis cell made of a quartz tube and two quartz windows glued to each end with a volume of 16 cm$^3$ (PLC) following the design of Pollack et al. (2010). Aluminium foil is wrapped around the quartz tube to increase the reflectivity to give the highest conversion efficiency of $NO_2$. The diodes are placed at each end of the quartz tube, as shown in Figure S2, without touching the windows to avoid increases in the temperature when the diodes turn on. BLCs have been used at the CVAO since the instrument was installed in 2006, with the most recent converter installed in April 2015 (a BLC2 model), where the wavelength was changed to 385 nm from 395 nm. The PLC was installed in March 2017. The air flow through the instrument is controlled at ~1000 sccm by a mass flow controller (MKS, M100B) giving a residence time of 0.96 s through each of the converters.

160   To measure NO and $NO_x$ (NO + $NO_2$ converted into NO) the air is introduced to the

161  chemiluminescent detector (CLD), where NO is oxidized by excess $O_3$ into excited $NO_2$ in the

162  reaction volume (241 mL, aluminium with gold coating (Ridley and Grahek, 1990)) shown in

163  Figure 2. The reaction volume is kept at low pressure to minimize quenching of excited $NO_2$

164  and thereby maximize the NO chemiluminescence lifetime. The photons emitted from the

165  excited $NO_2$ molecules when they relax to ground state are detected by the PMT (Hamamatsu

166  R2257P) to give a signal for NO. $NO_2$ is converted into NO by the BLC for 1 minute, and then

167  the PLC for 1 minute, each period producing a signal due to NO + $NO_2$. The signal detected

168  by the PMT ($S_M$) is caused by NO reacting with $O_3$ ($S_{NO}$), dark current from the thermionic

169  emissions from the photocathode of the PMT ($S_D$), and an interference ($S_I$) which can be due

170  to $O_3$-surface reactions that cause light emissions in the reaction cell, other gas-phase reactions

171  creating chemiluminescence, and from illumination of the chamber walls during $NO_2$

172  conversion (Drummond et al., 1985; Reed et al., 2016):

173    $S_M = S_{NO} + S_D + S_I$             (I)

174   The PMT is cooled to -30°C to reduce the dark current, giving the instrument a higher

175  precision. Other molecules in the atmosphere such as alkenes also react with ozone and emit

176  photons to reach their ground state, but at a different time-scale to that of $NO_2$ (Alam et al.,

177  2020; Finlayson et al., 1974). This can give an interfering signal causing the NO and $NO_x$

178  mixing ratios to be overestimated. However, most of these reactions emit photons at 400-600

179  nm and are therefore filtered by a red transmission cut-off filter (Schott RG-610) placed in

180  front of the PMT (Alam et al., 2020). The filter transmits photons with a wavelength higher

181  than 600 nm (Drummond et al., 1985). A background measurement is therefore required to

182  account for the dark current of the PMT, $O_3$-surface reactions, and for the remaining interfering

183  reactions occurring at a different time-scale to that of $NO_2$. Background measurements are

184  made by allowing ambient air to interact with $O_3$ in the zero volume (180 mL, PFA, Savillex,

185  LLC) before reaching the reaction volume (Figure 2). Most excited $NO_2$ molecules will reach

186  their ground state before the sample reaches the PMT, meaning the signal from NO will not be

187  measured. The efficiency of the reaction between NO and $O_3$ in the zero volume is calculated

188  from the calibration, asnd will be explained in section 2.4.3. Background measurements are

189  performed every 5 minutes to take changing ambient conditions such as humidity into account,

190  which can affect the background signal for example via the quantity of light emitted from

191  interference reactions ($S_I$).

NO, NO$_2$ and the background signal are all detected on the same channel, and the instrument cycle is 1 min of background, 2 min of NO (when the NO$_2$ converters are off), 1 min of BLC NO$_x$ (the BLC converter is on), and 1 min of PLC NO$_x$ (the PLC is on).

## 2.4 Calibration

Prior to June 2019, calibrations were performed every 73 hours by standard addition in order to account for temperature and humidity changes in the ambient matrix. In June 2019 the calibration frequency was changed to every 61 hours to ensure that during any given month, calibrations are carried out for approximately equal periods during the night and the day. To calibrate the NO sensitivity, 8 sccm of 5 ppmᵥ NO calibration gas in nitrogen is added to the ambient air flow of ~1000 sccm, giving an NO mixing ratio of approximately 40 ppbᵥ. The mixing ratio used for calibrations are approximately 10,000 times that of the ambient measurements, however, due to reduced cylinder stability for lower NO mixing ratios it is difficult to calibrate at much lower mixing ratios and the chemiluminescence is expected to be linear across the range of expected mixing ratios (Drummond et al., 1985). The calibration gas is added between the PTFE filter and the NO$_2$ converter as shown in Figure 2. The conversion efficiency of the BLC and the PLC is calibrated by gas phase titration (GPT), where oxygen is added to the sampled NO calibration gas before entering the titration cell, which contains a UV lamp that converts oxygen to ozone. Between 60-80% of the NO calibration gas is oxidized into NO$_2$, giving a known mixing ratio of NO$_2$. A theoretical calibration sequence is shown in Figure 3. The first cycle is to calibrate the sensitivity and the second is to calibrate the NO$_2$ conversion efficiency.  Each actual calibration includes three cycles of sensitivity calibration and two cycles of conversion efficiency calibration. The signal from NO$_2$ observed in the NO sensitivity calibration is due to traces of NO$_2$ in the calibration gas. Figure S3 shows the observed percentage of NO$_2$ in the calibration cylinders from January 2014 to August 2019 calculated from the measured sensitivity (sec. 2.4.1) and the conversion efficiencies (CE) of the two converters (sec. 2.4.2):

$$\text{NO}_2 \text{ in cylinder (ppt} V \text{ppt)} = \frac{(\text{NO.c}_{(1)} - \text{NO}_{(1)})}{\text{Sensitivity} \times \text{CE}} \tag{II}$$

$$\text{Percentage NO}_2 = \frac{\text{NO}_2 \text{ in cylinder}}{\text{NO}_2 \text{ in cylinder} + \text{NO cal conc.}} \tag{III}$$

221   The percentage is stable for both converters, however, the PLC shows approximately 3-
222   4% $NO_2$ in the NO calibration gas compared to 5-10% for the BLC, which is caused by a BLC
223   artefact. The cylinders used were certified to $\leq 2\%$ $NO_2$.

224

## 225   2.4.1 Sensitivity

226   The sensitivity of the instrument is calculated from the increase in counts per second
227   caused by the calibration gas during NO calibration (untitrated, i.e. without $O_3$) and from the
228   mixing ratio of the calibration gas as shown by equation (IV). The NO counts per second from
229   the previous measurement cycle before the calibration is subtracted to give the increase due to
230   the calibration gas. The previous cycle needs to be stable and low in NO to give an accurate
231   sensitivity, which is the case at the CVAO.

232   $$\text{Sensitivity} = \frac{\text{Counts per second during calibration} - \text{Counts per second in previous cycle}}{\text{Mixing ratio of calibration gas}} \qquad \text{(IV)}$$

233   The sensitivity of the instrument depends on the pressure of the reaction chamber, the
234   ozone mixing ratio in the reaction chamber, the flow of the sample through the reaction
235   chamber, and the temperature of the reaction chamber. To maintain a stable sensitivity, all four
236   parameters should be kept stable (Galbally, 2020). From January 2014 to August 2019 the
237   sensitivity has varied between 2.7 and 7.4 counts $s^{-1}$ ~~pptV~~ppt$^{-1}$ with changes of less than 5%
238   between subsequent calibrations (see Figure S4), unless the instrument has been turned off for
239   a long period of time due to instrumental problems.

240

## 241   2.4.2 Conversion Efficiencies

242   The conversion efficiency of the BLC and the PLC is calculated based on the titrated (with
243   added $O_3$) and the untitrated (without added $O_3$) NO calibration gas as described in equation
244   (V). The numerator gives how much of the NO is titrated into $NO_2$ and the denominator
245   represents the $NO_2$ measured when taking the $NO_2$ content in the NO calibration gas into
246   account. In equation (V), "NO" is the measurement of only NO i.e. when the converters are
247   off, NO.c is when one of the converters are on therefore the measurement is $NO + NO_2$ and (1)
248   and (2) represent untitrated and titrated NO, respectively.

249   $$CE = \frac{[(NO.c_{(2)} - NO_{(2)}) - (NO.c_{(1)} - NO_{(1)})]}{[NO_{(1)} - NO_{(2)}]} = 1 - \frac{NO.c_{(1)} - NO.c_{(2)}}{NO_{(1)} - NO_{(2)}} \qquad \text{(V)}$$

250 The conversion efficiency of the BLC has varied from 82% to 91% between its installation in
251 April 2015 and August 2019 ($j$ ~3 s$^{-1}$). Prior to April 2015, an older generation BLC ($\lambda$ = 395
252 nm) with a conversion efficiency of 30-35% was used ($j$ ~0.5 s$^{-1}$). The conversion efficiency
253 of the PLC has varied between 50% and 55% from its installation in March 2017 to August
254 2019 ($j$ ~1 s$^{-1}$). See Figure S5 for all the calculated conversion efficiencies.

255

### 2.4.3 Efficiency of the Zero Volume

257 Background measurements are made by reacting NO and interference compounds with $O_3$
258 in the zero volume (Figure 2). The system is set up so that $NO_2$ produced from NO will relax
259 to the ground state before it is measured in the downstream reaction chamber, whereas it is
260 assumed that any interfering compounds will emit photons when reaching the reaction chamber
261 and be measured as a background signal (Drummond et al., 1985; Galbally, 2020). If the zero
262 volume is too small or the $O_3$ mixing ratio is too low, some untitrated NO may lead to $NO_2$
263 chemiluminescence within the reaction chamber and the background will be overestimated. On
264 the other hand, if the zero volume is too large, some of the interfering compounds may have
265 relaxed to their ground state before the reaction chamber and the background signal will be
266 underestimated. The residence time of zero volume is 10.8s compared to 14.5s for the reaction
267 volume. The efficiency of the zero volume can be calculated from the calibration cycle. The
268 difference in background counts from before a calibration cycle to during the calibration cycle
269 shows how much of the added NO from the calibration cylinder does not react with $O_3$ in the
270 zero volume. By dividing this difference by the signal due to NO during the NO measurement
271 of the calibration cycle, which is obtained by subtracting the NO measurement from the
272 previous measurement cycle, the inefficiency of the zero volume is obtained. The efficiency is
273 determined for each calibration cycle (eq. VI) and plotted in Figure S6. It is consistently above
274 98%.

275 $$\text{Efficiency}_{ZV} = 1 - \frac{\text{cal zero} - \text{measurement zero}}{\text{NO cal} - \text{previous NO cycle}} \qquad \text{(VI)}$$

276

### 2.4.4 Artefact Measurements

278 As described in section 2.3, $NO_x$ measurements may have artefacts from
279 chemiluminescence caused by interfering gas-phase reactions and/or from compounds

produced by illumination of the reaction chamber walls as well as from pressure differences in the instrument (Drummond et al., 1985; Reed et al., 2016). To estimate artefacts, it is necessary to measure the signal from $NO_x$-free air. The calibration sequence is followed by sampling $NO_x$-free air generated from a pure air generator (PAG 003, Eco Physics AG) for 30 minutes. According to the manufacturer, the PAG not only scrubs NO, $NO_2$ and $NO_y$ from the ambient air but also $SO_2$, VOCs, $H_2O$ and $O_3$. An overflow of PAG air is introduced between the aerosol filter and the $NO_2$ converters as shown in Figure 2 and the cycle of background, NO, $NO_x$ BLC, and $NO_x$ PLC is used to estimate artefact NO and $NO_2$ measured by the instrument. The artefacts are estimated using the sensitivity and conversion efficiencies measured in ambient air, where humidity is expected to be higher. This could cause the artefacts to be either under- or overestimated.

## 2.4.4.1    NO Artefact

The NO artefact can be caused by two things; alkenes reacting with $O_3$ and giving chemiluminescence above 600 nm at approximately the same rate as $NO_2$ or a difference in pressure between the zero volume and the reaction volume. An artefact caused by alkenes will be positive and overestimate the NO mixing ratio, where an artefact due to a pressure difference can be either negative or positive. It can be estimated as the offset from 0 ~~pptV~~ppt when the mixing ratio sampled is 0 ~~pptV~~ppt. The NO mixing ratio is expected to be 0 ~~pptV~~ppt when sampling $NO_x$-free air or between 22.00 and 04.00 UTC at night. NO generated during the day is rapidly oxidized into $NO_2$ through reactions with $O_3$ and $RO_2$ after sunset. During the night, NO is not generated from photolysis of $NO_2$, and there are no significant local sources of NO at Cabo Verde when the air masses come from over the ocean (which is >95% of the time). The average NO mixing ratio between 22.00 and 04.00 UTC and the average NO mixing ratio from the PAG zero air tend to be very similar, with the PAG artefact (-3.7~~68~~ ± 22.9~~1~~ ~~pptV~~ppt (2σ), January 2014 – August 2019) ~~generally~~ordinarily lower than the night time artefact (0.4~~39~~ ± 11.9~~2~~ ~~pptV~~ppt (2σ), January 2014 – August 2019). Time series of both NO artefact measurements can be found in Figure S7 in the supplementary information. The night time NO artefact is used as it is measured more frequently, it contains the same ambient matrix with nothing scrubbed and to eliminate the possibility of residual NO influencing background measurements determined from the PAG. Since the PAG scrubs VOCs it will also not give an estimate of the artefacts caused by fast reacting alkenes.

312

## 2.4.4.2    NO$_2$ Artefact

NO$_2$ converters have previously been shown to have artefacts caused by thermal or photolytic conversion of reactive nitrogen compounds (NO$_z$) other than NO$_2$ as well as illumination of the chamber walls (Drummond et al., 1985; Reed et al., 2016; Ryerson et al., 2000). Fast reacting alkenes, which can cause overestimations of the NO mixing ratios, will not cause the NO$_2$ mixing ratio to be overestimated, since the NO signal is subtracted from the NO$_2$ signal.

The spectral output of an NO$_2$ converter with a wavelength of 385 nm was compared to absorption cross sections of NO$_2$ and potential interfering species such as BrONO$_2$, HONO and NO$_3$ (Reed et al., 2016). The photolytic converteor was shown to have good spectral overlap with the NO$_2$ cross section with minimal spectral overlap with other NO$_z$ species, except for a small overlap with the absorption cross section of HONO. The interference from BrONO$_2$, HONO and NO$_3$ have additionally been evaluated previously for a similar set-up using a Hg lamp (Ryerson et al., 2000). At equal concentrations of NO$_2$ and NO$_z$ species, BrONO$_2$ and NO$_3$ were estimated to maximum have an interference of 5% and 10%, respectively, using a lamp with a wider spectral overlap with the interfering species than what is observed for the LEDs used at the CVAO (Ryerson et al., 2000). At the CVAO, HONO levels have previously been measured to peak at ~3.5 pptVppt (at noon; (Reed et al., 2017)). For the typical Gaussian output of a UV-LED this interference is calculated to be 2.0, 12.6, and 25.7% for UV-LEDs with principle outputs of 395, 385, and 365 nm respectively, resulting in a maximum interference of <0.5 pptVppt during peak daylight hours. Photolytic conversion of NO$_z$ species is therefore not expected to be an important contributor to the NO$_2$ artefact at the CVAO due to the narrow spectral output of the LEDs.

Each converter is only on for 1 minute in a 5-minute cycle. For thermal conversion to be a major contributor to the artefact, the converter would have to increase in temperature during that one minute and not the rest of the cycle otherwise an increase in signal should be constant since the air continues to flow through the converters when they are turned off. Thermal decomposition of NO$_z$ species is therefore not expected to have an effect in a climate like the one in Cabo Verde, where the sample temperatures are similar to the ambient temperatures.

342    It has been shown that the walls of a BLC made out of a porous Teflon-like doped block

343    becomes contaminated from the ambient air over time, and when the walls are illuminated

344    reactions take place on the surface causing an artefact (Reed et al., 2016; Ryerson et al., 2000).

345    The BLC is similar to the one used by Reed et al. (2016) and it is therefore expected to have

346    an artefact due to reactions taking place on the surface. The PLC is not expected to be

347    contaminated in the same way as it does not have porous chamber walls.  Ryerson et al. (2000)

348    observed an increase in artefact over time when sampling ambient air for a similar PLC,

349    however, this is not observed for the PLC in the very clean environment at the CVAO (0-10

350    ~~pptV~~ppt between August 2017 and August 2019, see below) and surface reactions are therefore

351    expected to give a negligible artefact for the PLC.

352    The total artefact can be determined by measuring the $NO_2$ signal when the $NO_2$ mixing

353    ratio is 0 ~~pptV~~ppt, however, it is virtually impossible to scrub all $NO_x$ from the ambient air and

354    nothing else. To estimate the $NO_2$ artefact, PAG zero air is measured using both converters.

355    The PLC measures between 0-10 ~~pptV~~ppt compared to 10-60 ~~pptV~~ppt using the BLC. Since,

356    as discussed above, the $NO_2$ artefact of the PLC is assumed~~believed~~ to be negligible, the

357    ~~signal~~measurement of PAG zero air by the PLC is assumed~~believed~~ to represent the remaining

358    $NO_2$ in the zero air after scrubbing. If the PLC does have an artefact, then both $NO_2$

359    measurements will be overestimated by the amount of this artefact. The signal from the BLC

360    when measuring PAG zero air is expected to be due to the illumination of the chamber walls

361    in addition to the traces of $NO_2$ left in the zero air. The artefact due to wall reactions in the

362    BLC can therefore be estimated by subtracting the signal measured by the PLC.

363

# 3  Data Analysis

365    Time periods with known problems such as maintenance on the manifold, ozone leaks,

366    and periods when the PMT has not reached $<-28°C$ are not included in the dataset. The mean

367    and standard deviation of the zero (background), NO, $NO_2$ BLC and PLC are determined for

368    each 5-minute measurement cycle.  To avoid averaging over the time it takes the detector to

369    change and stabilize between the different types of measurements, the last 50 seconds of the

370    measurement cycle are used for the background and the NO counts, and the last 30 seconds for

371    the BLC $NO_x$ and the PLC $NO_x$ counts.  Each cycle is filtered based on the percentage standard

372    deviations and differences in counts between subsequent cycles. If the standard deviation or

373    the difference in counts are outside the mean $\pm 2\sigma$ (see Table 1) calculated from a 5-year period

374 between 2014 and 2018, the cycle is not used for further analysis. This removes noisy data as
375 well as sharp spikes but keeps data with sustained increases lasting more than 5 minutes.

376 To obtain the signals due to NO and $NO_2$, the interpolated zero and NO measurements are
377 subtracted from the NO and $NO_x$ measurements, respectively. They are converted to a
378 concentration by using the interpolated sensitivity and conversion efficiency as shown in
379 equation VII and VIII:

380 $$\text{NO mixing ratio} = \frac{\text{NO measurement} - \text{background measurement}}{\text{Sensitivity}} \qquad \text{(VII)}$$

381 $$\text{NO}_2 \text{ mMixing ratio} = \frac{\text{NO}_x \text{ measurement} - \text{NO measurement}}{\text{Sensitivity} \times CE}$$

382     (VIII)

383 The NO and $NO_2$ BLC concentrations are corrected by subtracting the interpolated
384 artefacts described in sections 2.4.4.1 and 2.4.4.2. If the difference between two subsequent
385 NO artefact measurements vary by more than the mean $\pm 2\sigma$ of the differences in NO artefacts
386 determined from January 2014 – August 2019 ($0.00 \pm 6.2\text{18 pptV}$ppt), the measurements made
387 between ~~will~~are not ~~be~~ used for further analysis due to a potential step change between the
388 determinations.

389 Hourly averages of all the measurements are determined. If data coverage during the hour
390 is less than 50%, the hour is flagged and discarded from the data analysis. The hourly $NO_x$ (NO
391 + $NO_2$ PLC) concentrations between June 2017 and August 2019 are plotted as a function of
392 wind speed and direction in figure 4. It can be observed that the concentrations are enhanced
393 at low wind speed and when the air crosses the island (from the southwest). Measurements
394 made at a wind speed <2 m/s or from a wind direction ~~>100~~-360° are, therefore, flagged as
395 suspected of local contamination and are not used in the analysis. Extreme mixing ratios outside
396 the mean $\pm 4\sigma$ of the 5-year for NO and 2-year period for $NO_2$ are flagged as suspicious (see
397 Table 1 for boundaries). Lastly, inconsistence in the measurements such as differences outside
398 the mean $\pm 4\sigma$ between the mean and median of a measurement (see Table 1 for boundaries)
399 and differences between the two $NO_2$ measurements are flagged as suspicious ($0.4 \pm 32.2$
400 ~~pptV~~ppt). The data remaining after these removals are 88% of the original NO and $NO_2$ BLC
401 dataset and 83% of the $NO_2$ PLC dataset remain to analyse.

402

## 3.1 Corrections

As described above, excited $NO_2$ can be quenched by other sampled molecules, giving a lower observed mixing ratio than the real value. Water molecules are effective quenchers and therefore a correction is usually applied depending on the humidity (Matthews et al., 1977; Ridley et al., 1992). However, since the calibrations at the CVAO are performed by standard addition, and a Nafion dryer is placed in front of the instrument, this is not necessary.

Additionally, NO can react with $O_3$ in the ambient air in the inlet and manifold giving an overestimation of $NO_2$ and an underestimation of NO. To correct for this the following equations are used (Gilge et al., 2014):

$$[NO]_0 = [NO]_{E1} \times e^{k_{O_3} \times t_{E1}} \tag{IX}$$

$$[NO_2]_0 = \left( \frac{J_C + k_{O_3}}{J_C} \right) \times \left( \frac{[NO]_{E2} - [NO]_{E1} \times e^{-\left( k_{O_3} \times (t_{C2} - t_{C1}) + J_C \times t_{C2} \right)}}{1 - e^{\left( -\left( k_{O_3} + J_C \right) \times t_{C2} \right)}} \right) - [NO]_0 \tag{X}$$

where $[NO]_0$ is the corrected NO mixing ratio, $[NO]_{E1}$ is the uncorrected NO mixing ratio, $[NO_2]_0$ is the corrected $NO_2$ mixing ratio, $[NO]_{E2}$ is the uncorrected NO mixing ratio when the converter is on, $k_{O_3}$ is the rate of the reaction between NO and $O_3$ ($k(O_3+NO) \times [O_3] \times 10^{-9} \times$ M), $t_{E1}$ is the sum of the residence time from the inlet to entry of the converter and the time the air is in the converter, $t_{C1}$ and $t_{C2}$ are the time the air is in the converter when the converter is on and off, respectively, and $J_C$ is the photolysis rate inside the converter. The residence time from the inlet to the entry of the converter has been 2.3 s since 2015 and the time the air is in each of the converters is 1.0 s (with and without the converter on). The $O_3$ mixing ratio measured at the CVAO has varied between 5 and 60 ppb~~V~~ (with an uncertainty of 0.07 ppb~~V~~) between 2014 and 2019. The ozone correction is calculated for each hour using a rate coefficient of $1.8 \times 10^{-14}$ cm$^3$ molecule$^{-1}$ s$^{-1}$ at 298K (Atkinson et al., 2004). This gives an average $O_3$ correction $\pm 2\sigma$ of $6.8 \pm 3.0\%$, $1.7 \pm 11.0\%$, and $1.3 \pm 7.1\%$ for NO, $NO_2$ BLC, and $NO_2$ PLC, respectively, when the mixing ratio measured is above 0.1 ~~pptV~~ppt (See supplementary information for an example of the calculation). Thus, at the low mixing ratios of $O_3$ present at Cabo Verde and the short residence time for sampling, the corrections for $O_3$ are well within the noise of the measurements (see below), but are still included in the final calculated mixing ratios.

# 4 Uncertainty Analysis

To be able to evaluate the $NO_x$ measurements made at the CVAO an extensive uncertainty analysis is performed. A summary of the analysis can be found in Table 2 and a detailed description in the supplementary information. The hourly precision and uncertainty of the instrument are estimated to characterize the uncertainties at the 95 percent confidence interval (Bell, 2001). The hourly precision is estimated from the zero count variability, which is directly related to the photon-counting precision of the PMT. The uncertainty of the hourly measurements is estimated by combining all the uncertainties associated with the measurements. This includes uncertainties in the calibrations, artefact determinations, and $O_3$ corrections as well as the precision of the instrument. The precision of the NO and $NO_2$ measurements are both included in the total uncertainty of the $NO_2$ measurements as the NO measurements are subtracted from the $NO_2$ measurements. Each term is converted into ~~pptV~~ppt to be able to combine them using error propagation.

The $2\sigma$ precision for hourly averaged NO data between January 2014 and August 2019 is 1.0~~0.96~~ ± 0.89 ~~pptV~~ppt. The hourly precisions reported here are in good agreement with our previously reported $1\sigma$ precision of the instrument of 0.30 ~~pptV~~ppt (Reed et al., 2017) and the $2\sigma$ precision of 0.6-1.7 ~~pptV~~ppt (Lee et al., 2009). The $NO_2$ precisions are determined by taking the conversion efficiency of the respective converters into account. The hourly $2\sigma$ precision for hourly averaged $NO_2$ data between March 2017 and August 2019 becomes 1.4~~5~~ ± 0.8~~2~~ ~~pptV~~ppt and 2.7~~4~~ ± 2.2~~18~~ ~~pptV~~ppt for the BLC and PLC, respectively. The determined $NO_2$ precisions are within the interval of previously reported precisions for the same instrument (Lee et al., 2009; Reed et al., 2017).

The total hourly uncertainty for each of the three measurements are determined by combining all the uncertainties described using propagation of uncertainties. The precisions are already calculated as hourly precisions in ~~pptV~~ppt. The calibration uncertainties are interpolated between each calibration and multiplied by the hourly concentrations of NO and $NO_2$ to calculate hourly uncertainties in ~~pptV~~ppt. The artefact uncertainties are interpolated between each artefact determination, and the uncertainty due to ozone corrections is determined by multiplying the % uncertainties by the hourly concentrations of NO and $NO_2$. The hourly uncertainties are determined to be 1.4~~2~~ ± 1.5~~47~~ ~~pptV~~ppt, 8.4~~38~~ ± 7.5~~46~~ ~~pptV~~ppt, and 4.4~~4~~ ± 5.8~~79~~ ~~pptV~~ppt for NO, $NO_2$ BLC, and $NO_2$ PLC, respectively.

# 5 Results: Examples of Data

The first year of data (August 1$^{st}$ 2017 to July 31$^{st}$ 2018) is chosen as an example of the resulting NO and NO$_2$ datasets. October 2017, December 2017, and April 2018 are used to highlight the seasonality in the mixing ratios observed during a year of measurements. Panel A in figure 5 and 6 show the full O$_3$ corrected time series for NO and NO$_2$, respectively. Panel B, C, and D in the two figures show the time series for the three chosen months and panel E, F, and G show the 3-hour rolling average diurnals for the same months. Monthly diurnals for NO and NO$_2$ for the entire year can be found in figure S9~~8~~ and S10~~9~~, respectively.

Clear seasonality can be observed in the diurnal cycles of NO measurements with a maximum of ~10 ~~pptV~~ppt in Winter and a minimum of ~2 ~~pptV~~ppt in the spring and summer. This is in good agreement with that reported for previous years (Lee et al., 2009; Reed et al., 2017). The two NO$_2$ measurements are in general in good agreement when looking at the time series in figure 6. Offsets of up to 10 ~~pptV~~ppt between the two measurements can be seen over some time periods (E.g. April, Panel D), which are most likely caused by the calculated BLC artefact for those periods either being too high or too low. This is supported by the diurnals having the same shape, but with an offset. Monthly diurnals of the two NO$_2$ measurements agree within 2 standard errors except in August 2017, where the offset between the two measurements is larger than for the remaining months. NO$_2$ shows a fairly flat diurnal signal, although a small increase in daytime NO$_2$ is evident in some months, which is in agreement with that reported for previous years (Lee et al., 2009; Reed et al., 2017). Spikes in the early morning are noticeable in the NO$_2$ diurnals for July-November, which correspond to the months with an average lower wind speed than the rest of the year (the diurnal for April also shows a spike, however, it is caused by data from~~only~~ one morning). These spikes could be caused by local fishing boats passing upwind of the observatory in the morning hours, which will give a more prominent spike a low wind speed. Monthly wind speed diurnals can be found in figure S11~~0~~. The good agreement between the two NO$_2$ measurements observed in figure 6 can also be observed in figure 7, where the two are plotted against each other. The data points are scattered around the 1:1 line shown in black ~~with an overestimation by the BLC~~. A linear least squares regression (with uncertainty in the BLC measurements) and ~~A~~an orthogonal distance regression (ODR) (with uncertainty in both measurements) are~~is~~ performed to evaluate the scatter of the data points with ~~uncertainty in both measurements~~ between August 2017 and 2019. The resulting regression line~~s~~ are~~is~~ displayed in red (BLC = 0.99 × PLC + 0.7 ppt) and blue (B~~P~~LC ~~NO$_2$~~= 1.08~~0.92~~ × B~~P~~LC – 0.6 ppt ~~NO$_2$, R$^2$ = 0.92~~). The deviation in the slope

17

497 from 1 for both regressions are consistent with the uncertainty in the measured $NO_2$ artefact

498 which has been determined to be 7.2 ± 7.2 ppt.

499

500     The seasonality of the NO measurements can be explained by a combination of the

501 variation of the origin of the air masses arriving at the CVAO, meteorology, photolysis rates,

502 and seasonality of emissions. Back trajectories of the three months used as examples are shown

503 in figure 8. FLEXPART version 10.4 is used in backwards mode, driven by pressure level data

504 from Global Forecast System (GFS) reanalyses at 0.5°×0.5° resolution (Pisso et al., 2019; Stohl

505 et al., 1998). 10-day back-trajectory simulations are initialised every 6 hours, releasing 1000

506 particles from the CVAO site. Further information on FLEXPART can be found in the

507 supplementary information. During the winter maximum (December) the back-trajectories

508 indicate that the air reaching CVAO is largely dominated by African air, compared to during

509 the spring minimum (April), which is dominated by Atlantic marine air.  Large west African

510 cities such as Dakar and Nouakchott, and/or the shipping lanes to the east/northeast of Cabo

511 Verde, are potential candidates for the source of elevated $NO_x$. The NO mixing ratios measured

512 in October are higher than those in April and lower than in December. This may be due in part

513 to the influence of polluted African air arriving at Cabo Verde, which is more prominent in

514 October than in April, but less so than in December. The $NO_2$ and the total $NO_x$ (NO + PLC

515 $NO_2$, figure 9) similarly show higher levels in December than April, but the mixing ratios

516 observed in October are similar to those in April. It should be noted that some of the days with

517 high percentages of African air have missing data or wind directions from other places than the

518 north east.

519     From table 3 it can be observed that the NO, $NO_2$, and $NO_x$ measurements at the CVAO

520 compare well to the few other measurements in the remote marine boundary layer as well as

521 background sites in Alert, Canada and measurements in the free troposphere.  A wintertime

522 seasonal increase in NO, $NO_2$, and $NO_x$ can be observed during December-February, which

523 corresponds to the months when surface air masses arrive at Cabo Verde from western Africa

524 (Carpenter et al., 2010; Lee et al., 2009).

525

## 6 Conclusion

NO$_2$ was measured at a remote marine site by photolytic conversion to NO followed by chemiluminesence detection, using two different methods for conversion. A photolytic NO$_2$ converter with external diodes and a quartz photolysis cell (PLC) has been installed at the Cape Verde Atmospheric Observatory and the NO$_2$ measurements have been compared to those of the historical BLC used at the site, which has internal diodes and a reaction chamber made of Teflon-like barium doped material. The two measurements show good agreement (BLC = 0.99 × PLC + 0.7 ppt, linear least squares analysis)~~(PLC NO$_2$ = 0.92 × BLC NO$_2$, R$^2$ = 0.92)~~ with small differences due to uncertainties in the estimations of the BLC NO$_2$ artefact. Even though the PLC has a lower conversion efficiency (CE= 52 ± 4%) than the BLC (CE= 85 ± 4%), it is preferred due to its assumed negligible artefact as a consequence of having non-porous/non-reactive walls. The assumption of a zero artefact causes the hourly uncertainty of the NO$_2$ measurements to be roughly halved. With 2σ hourly precisions of 1.0~~0.96~~ ± 0.8~~9~~ ~~pptV~~ppt, 1.45 ± 0.8~~2~~ ~~pptV~~ppt, and 2.7~~4~~ ± 2.2~~18~~ ~~pptV~~ppt and 2σ hourly uncertainties of 1.4~~2~~ ± 1.5~~47~~ ~~pptV~~ppt, 8.4~~38~~ ± 7.5~~46~~ ~~pptV~~ppt, and 4.4~~4~~ ± 5.8~~79~~ ~~pptV~~ppt for NO, NO$_2$ BLC, and NO$_2$ PLC, respectively, the instrument has a high repeatability and low uncertainties for all the measurements. The mixing ratios observed at the CVAO (NO: 2-10 ~~pptV~~ppt, NO$_2$: 5-50 ~~pptV~~ppt, and NO$_x$: 7-60 ~~pptV~~ppt at midday) are in good agreement with previous measurements at the CVAO as well as other ~~previous~~ remote measurements around the world.

## 7 Data availability

The processed data is available through Ebas (http://ebas.nilu.no/Pages/DataSetList.aspx?key=45DB99FE2B7F4F97864ECF800E71E5D5) and through CEDA (Center for Environmental Data Analysis, https://catalogue.ceda.ac.uk/uuid/d5422d54d519ed056cc17e97037732b8).

## 8 Author contribution

LN runs the instrument on a day-to-day basis. MW and STA wrote the script processing the data. MJR ran the back-trajectory analysis. BSN developed the photolytic converter setup. All authors were involved in the analysis, data evaluation and discussion of the results. STA wrote

556 the paper with contributions from all coauthors. All coauthors proofread and commented on
557 the paper.

558

## 9   Competing interests

560 The authors declare that they have no conflict of interest.

561

## 10   Acknowledgements

568

# 11 Tables

Table 1: Evaluation parameters of the measurements. When a measurement falls outside any of the intervals it will not be used for further data analysis. The mean ± xσ is calculated for 2014-2019 for the zero and NO measurements, and 2017-2019 for both $NO_2$ measurements. ~~The mean ± 2σ of the standard deviation and difference in counts/s between two subsequent measurement cycles.~~

| Measurement | Standard deviation of a measurement cycle (mean ± 2σ, %)[a] | Difference in counts/s between subsequent cycles (mean ± 2σ)[b] | Hourly mean ± 4σ~~Extreme values~~ (~~pptV~~ppt)[be] | ~~Extreme d~~Difference between mean and median (mean ± 4σ, ~~pptV~~ppt)[cd] |
|---|---|---|---|---|
| Zero | 2.4 ± 1.7 | - | - | - |
| NO | 2.5 ± 10.6 | 0 ± 515 | 1.7 ± 47.9 | 0.2 ± 4.1 |
| $NO_2$ BLC | 2.5 ± 7.5 | 0 ± 1432 | 16.8 ± 175.2 | 1.5 ± 33.0 |
| $NO_2$ PLC | 2.1 ± 2.5 | 0 ± 738 | 17.3 ± 176.8 | 1.7 ± 33.0 |

[a]The percentage standard deviation for each measurement cycle is ~~D~~determined as the standard deviation of a cycle divided by the mean of the same cycle. ~~[b]The difference in counts/s between each cycle.~~ [be]~~C~~Extreme measurements are determined to be mixing ratios, which are outside ~~alculated as~~ the hourly mean ± 4 standard deviations of the hourly mixing ratio. [cd]~~C~~Extreme differences between the hourly mean and median of the mixing ratios are ~~alculated~~determined ~~to be differences outside~~ ~~as~~ the hourly mean ± 4 standard deviations of the differences between the mean and median.

Table 2: Calculated uncertainties associated with the NO$_x$ measurements. The values in bold are the combined uncertainties for each type of measurement. Each uncertainty is given as the mean uncertainty ± 2 standard deviation of the data between January 2014 and August 2019 for NO and from March 2017 to August 2019 for both NO$_2$ measurements.

| Source of uncertainty | Probability distribution | Uncertainty (%) | Uncertainty (~~ppt~~√ppt) |
|---|---|---|---|
| Hourly precision/repeatability NO | Normal | | ~~1.00~~ 0.96 ± 0.89 |
| Hourly precision/repeatability NO$_2$ BLC | Normal | | 1.45 ± 0.82 |
| Hourly precision/repeatability NO$_2$ PLC | Normal | | 2.74 ± 2.~~21~~8 |
| Total Calibration uncertainty NO[a] | | 2.78 ± 8.05 | 0.03 ± 0.3~~27~~ |
| Total Calibration uncertainty NO$_2$ BLC[a] | | 3.44 ± 9.32 | 0.33 ± 1.3~~27~~ |
| Total Calibration uncertainty NO$_2$ PLC[a] | | 3.52 ± 8.67 | 0.43~~7~~ ± 1.3~~27~~ |
| Total NO artefact uncertainty[b] | | | 1.1~~05~~ ± 3.44 |
| Total NO$_2$ artefact uncertainty[b] | | | 7.2~~19~~ ± 7.24 |
| Hourly O$_3$ correction uncertainty NO | Normal | 20.00 ± 0.001 | 0.3~~27~~ ± 1.14 |
| Hourly O$_3$ correction uncertainty NO$_2$ BLC | Normal | 20.00 ± 0.001 | 2.5~~47~~ ± 6.8~~75~~ |
| Hourly O$_3$ correction uncertainty NO$_2$ PLC | Normal | 20.00 ± 0.001 | 2.6~~0~~ ± 6.4~~37~~ |
| **Total hourly uncertainty NO** | | | **1.4~~2~~ ± 1.5~~47~~** |
| **Total hourly uncertainty NO$_2$ BLC** | | | **8.4~~38~~ ± 7.5~~46~~** |
| **Total hourly uncertainty NO$_2$ PLC** | | | **4.44 ± 5.8~~79~~** |

[a]The individual uncertainties associated with the calibration can be be found in table S1. [b]The individual uncertainties associated with the artefact determination can be found in table S2.

Table 3: NO, NO$_2$, and NO$_x$ mixing ratios at different low NO$_x$ sites.

| | NO (pptv)[k] | NO$_2$ (pptv) | NO$_x$ (pptv) | Reference |
|---|---|---|---|---|
| **Tropospheric Marine** | | | | |
| CVAO, Cape Verde 2017-2018 | 2-10 | 5-50 | 7-60 | This study |
| Cape Grim, Australia[a] | 1-6 | 3-6 | 4-12 | (Monks et al., 1998) |
| SAGA3, Pacific Ocean, Cruise[b] | 2.9 ± 0.1 | | | (Torres and Thompson, 1993) |
| ASTEX, North Atlantic, Cruise[c] | 5 ± 4 | 29 ± 8 | | (Carsey et al., 1997) |
| WOCE, Indian Ocean, Cruise[d] | ~ 5 | 18-40 | | (Rhoads et al., 1997) |
| **Background Sites** | | | | |
| Alert, Canada[e] | 0.2-2.8 | 1.3-10.8 | | (Beine et al., 2002) |
| South Pole[f] | ~ 10 | | | (Jones et al., 1999) |
| **Free Troposphere** | | | | |
| Mauna Loa, USA[g] | 9.4 | 29.6 | 32 | (Carroll et al., 1992) |
| Pico Mountain, Portugal[h] | 0-9 | 19-30 | 20-37 | (Val Martin et al., 2008) |
| NASA GTE, Pacific Ocean, Aircraft[i] | ~ 1 | | | (Ridley et al., 1987) |
| Svalbard, Norway[j] | | | 27.7 ± 24.0 | (Beine et al., 1996) |

[a]Measurements made during the SOAPEX (Southern Ocean Atmospheric Photochemistry EXperiment) campaign during Austral summer in 1995. [b]Measurements from the Soviet-American Gases and Aerosols (SAGA) campaign between Hawaii and American Samoa between February and March. [c]Measurements from 6 clean days on the Atlantic Stratocumulus Transition Experiment (ASTEX). [d]Measurements from the World Ocean Circulation Experiment (WOCE) between South Africa and Sri Lanka. [e]Measurements made during 24-hour darkness and in spring. [f]Measurements made from January-March 1997 at the German Antarctic research station, Neumayer. [g]Measurements made during the Mauna Loa Observatory Photochemistry Experiment (MLOPEX) in May 1988. [h]Measurements made at Mount Pico between July 2002 and August 2005. [i]Measurements made in the upper marine boundary layer from 13 flights between California and west of Hawaii. [j]Measurements made at the Ny-Ålesund Zeppelin mountain station on Svalbard during a spring campaign in 1994. [k]Daytime values.
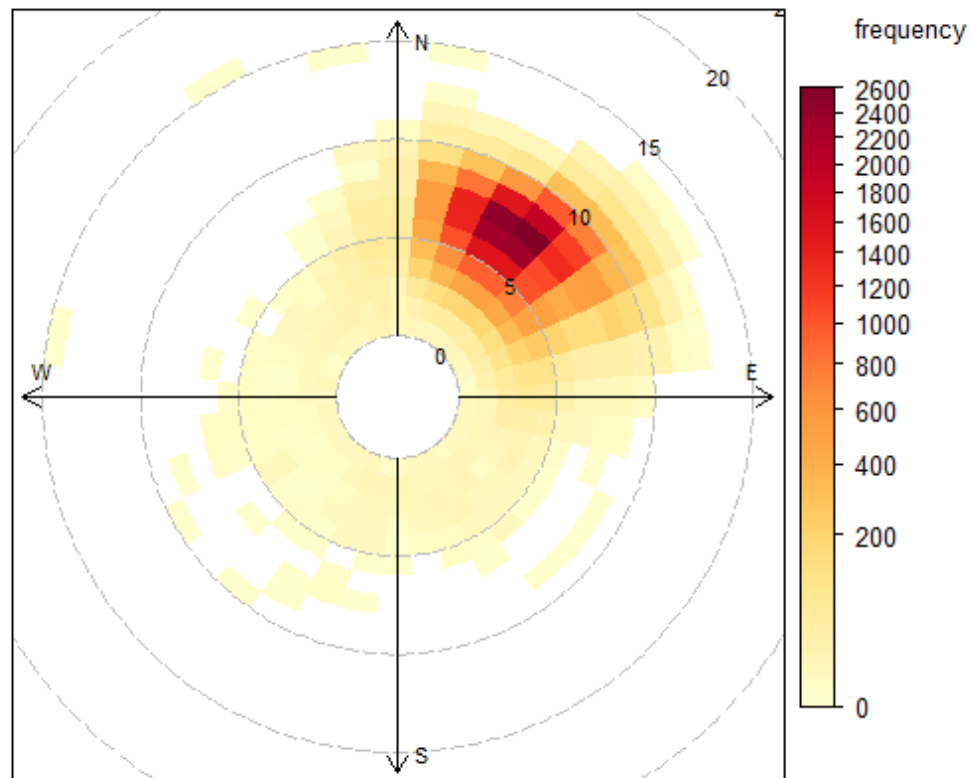
## 12 Figures

Figure 1: The frequency of hourly averaged wind speed and direction from January 2014 to August 2019. Each square symbolises 10 degrees of wind direction and 1 m/s wind speed. Each dashed circle shows an increase in wind speed of 5 m/s.
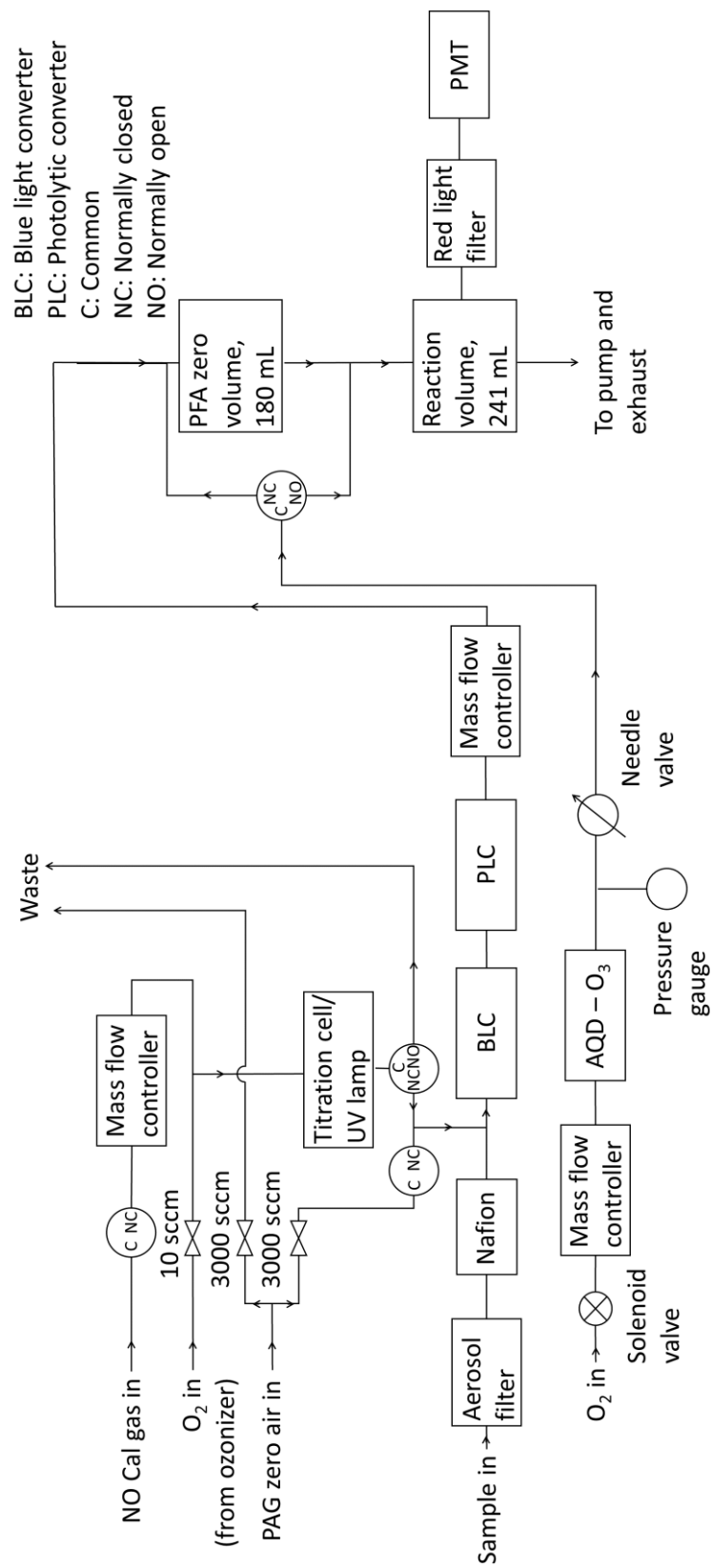
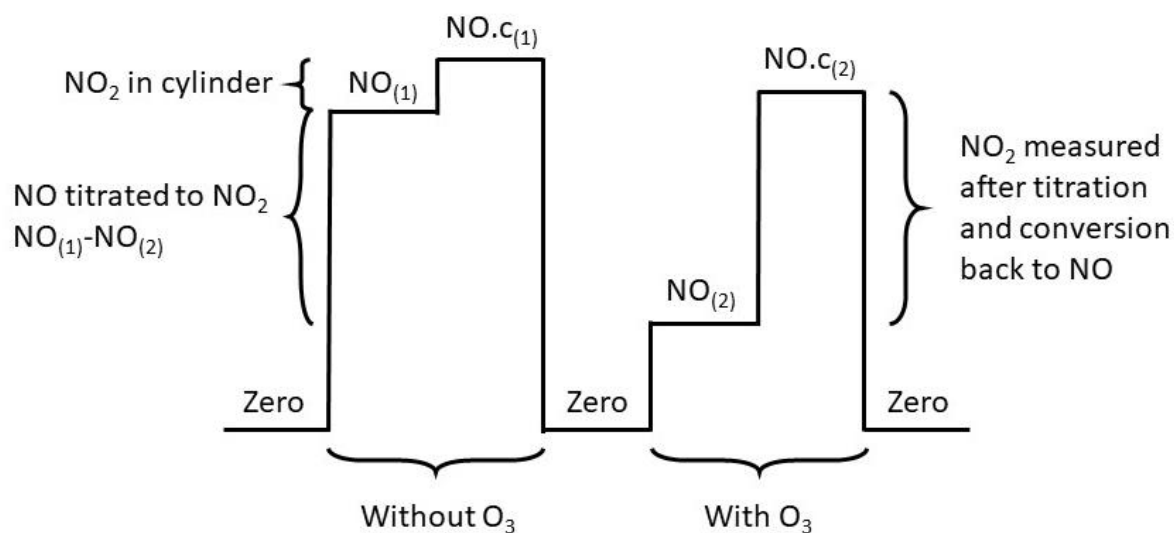Figure 2: Flow diagram of the NOx instrument at the CVAO.

Figure 3: A theoretical calibration cycle. "NO" is the measurement of only NO i.e. when the converters are off, NO.c is when one of the converters are on therefore the measurement is NO + $NO_2$ and (1) and (2) represent untitrated and titrated NO, respectively.
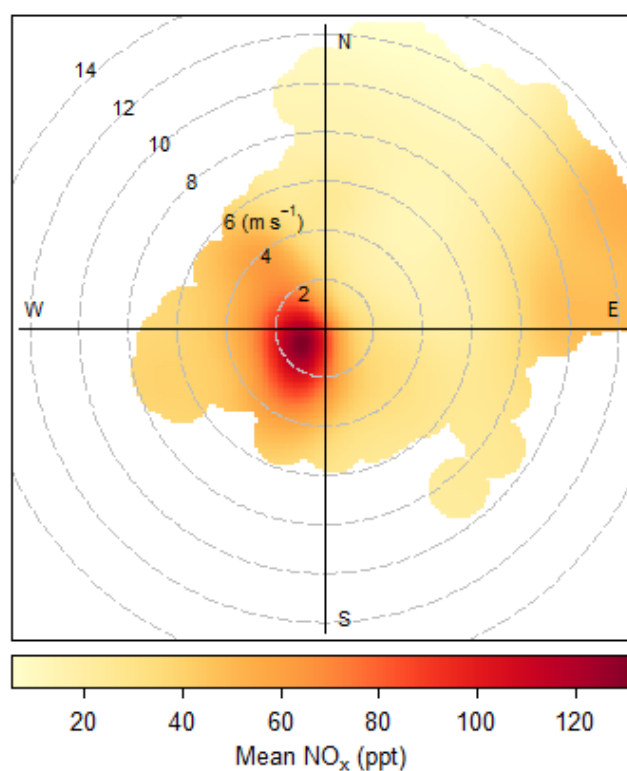


Figure 4: Total $NO_x$ from June 2017 to August 2019 plotted as a function of wind speed and direction.
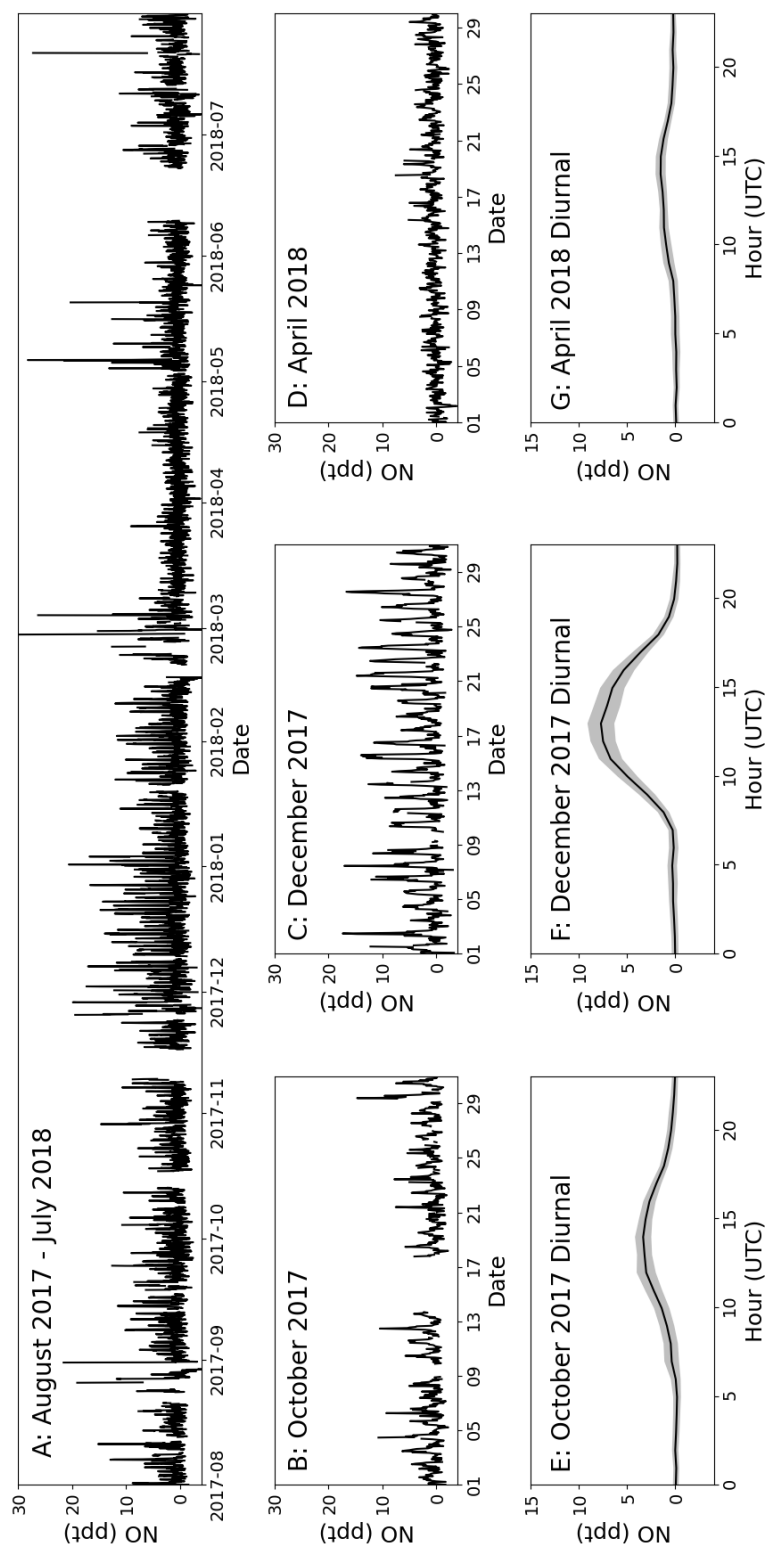
Figure 5: Panel A show the time series for filtered $O_3$ corrected NO from August 1st 2017 to July 31st 2018. Panel B, C and D zoom in on October 2017, December 2017 and April 2018, respectively. Panel E, F and G show the average diurnal of NO for October 2017, December 2017 and April 2018, respectively, with the coloured areas being ±2 standard errors. If there are less than 15 measurements available for the hour, it is not included in the diurnal.
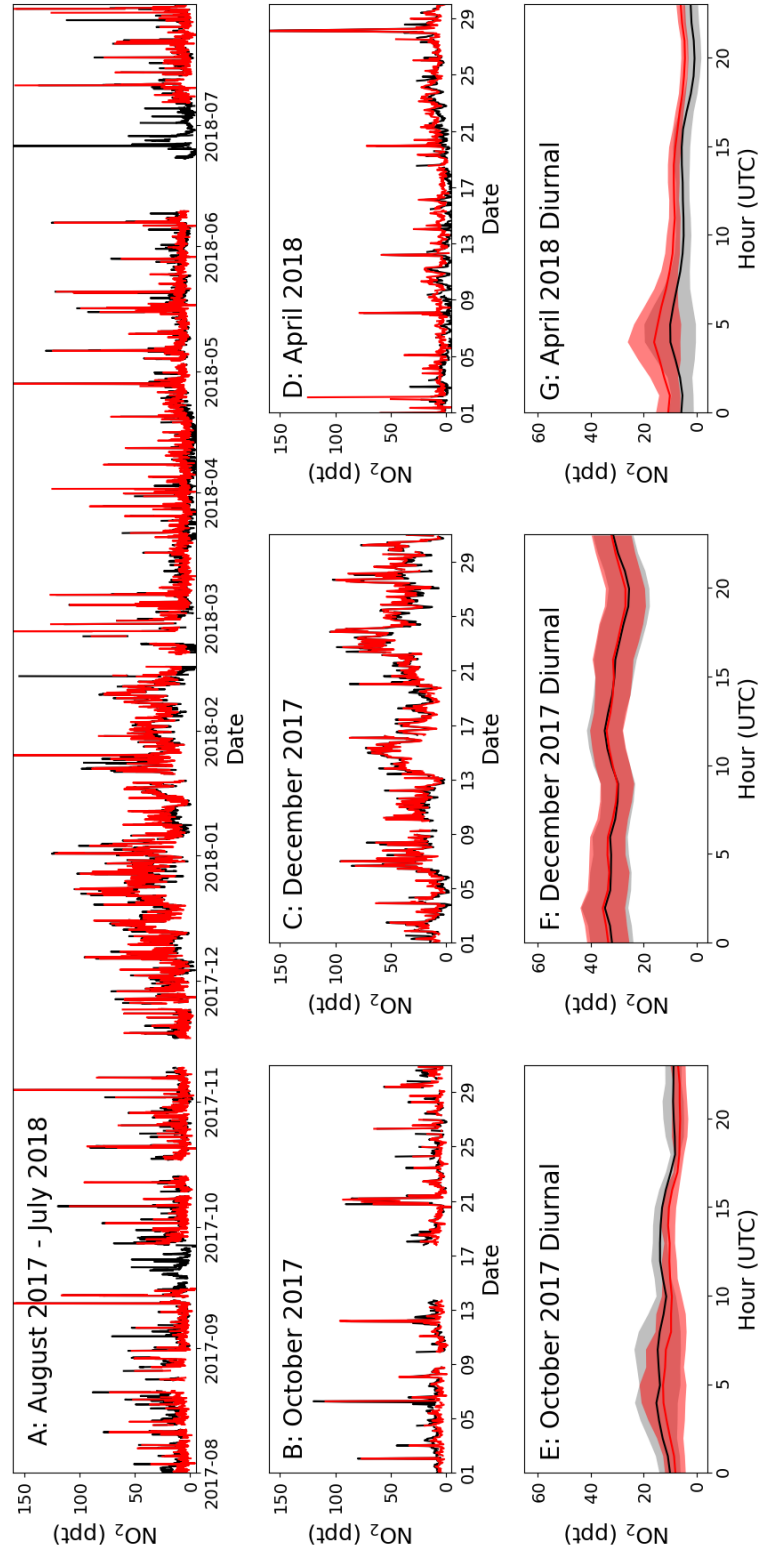
Figure 6: Panel A show the time series of filtered $O_3$ corrected $NO_2$ from August $1^{st}$ 2017 to July $31^{st}$ 2018 for the BLC (black) and PLC (red). Panel B, C and D zoom in on October 2017, December 2017 and April 2018, respectively, with the red line being the PLC and the black being the BLC. Panel E, F and G show the average diurnal of $NO_2$ for October 2017, December 2017 and April 2018, respectively, with the red line being the PLC and the black being the BLC and the coloured areas being $\pm 2$ standard errors. If there are less than 15 measurements available for the hour, it is not included in the diurnal.
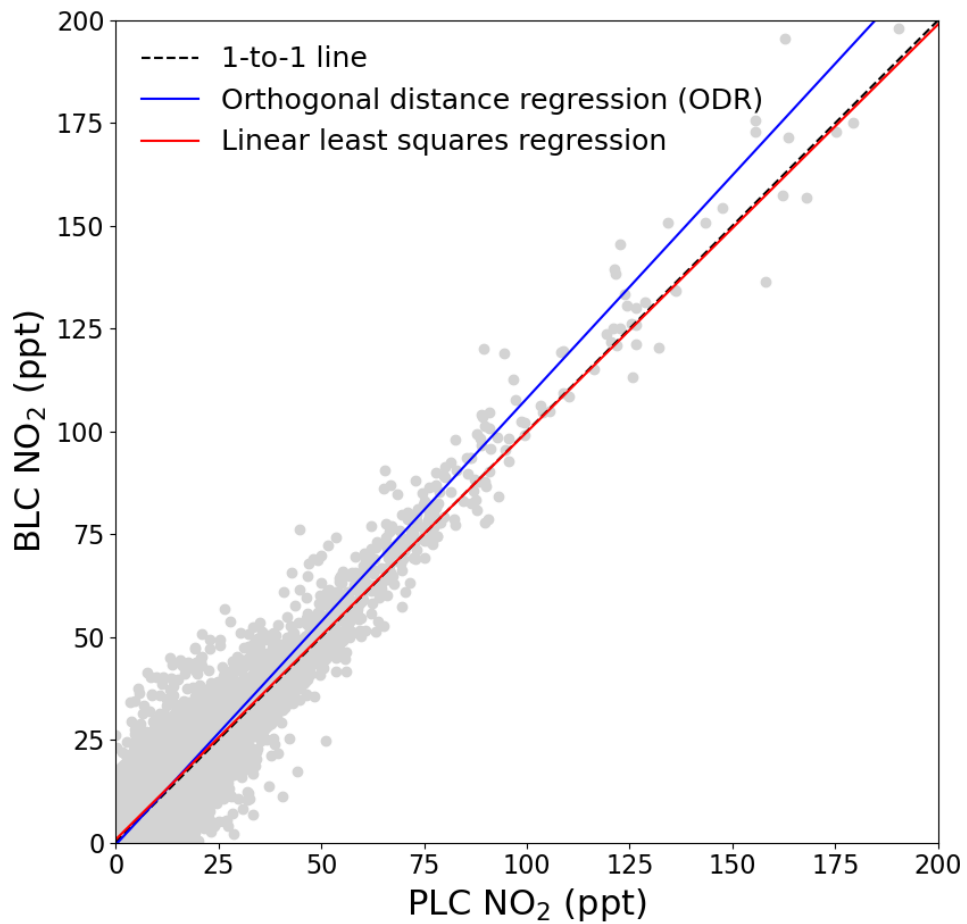
Figure 7: The ~~B~~PLC NO$_2$ mixing ratio~~concentration~~ is plotted against the ~~B~~PLC NO$_2$ mixing ratio~~concentration~~. The black dashed line~~s~~ shows the 1-to-1 relationship. The red line is the linear least square regression of the hourly data with uncertainty in y and the blue line is the orthogonal distance regression with uncertainties in both the x and y.
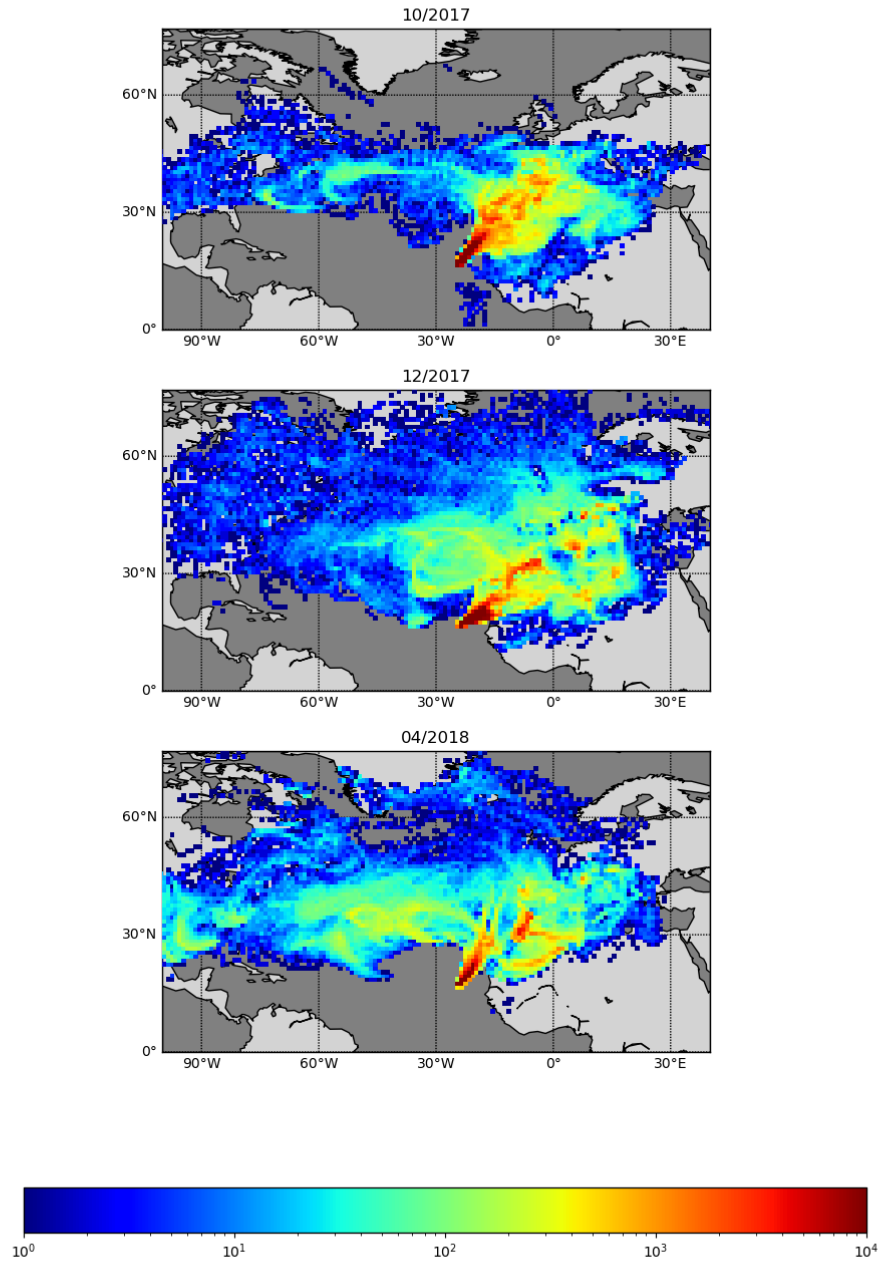
Figure 8: Back trajectories estimated for October 2017, December 2017, and April 2018. FLEXPART version 10.4 is used in backwards mode, driven by pressure level data from Global Forecast System (GFS) reanalyses at 0.5°×0.5° resolution (Pisso et al., 2019; Stohl et al., 1998). 10-day back-trajectory simulations are initialised every 6 hours, releasing 1000 particles from the CVAO site.
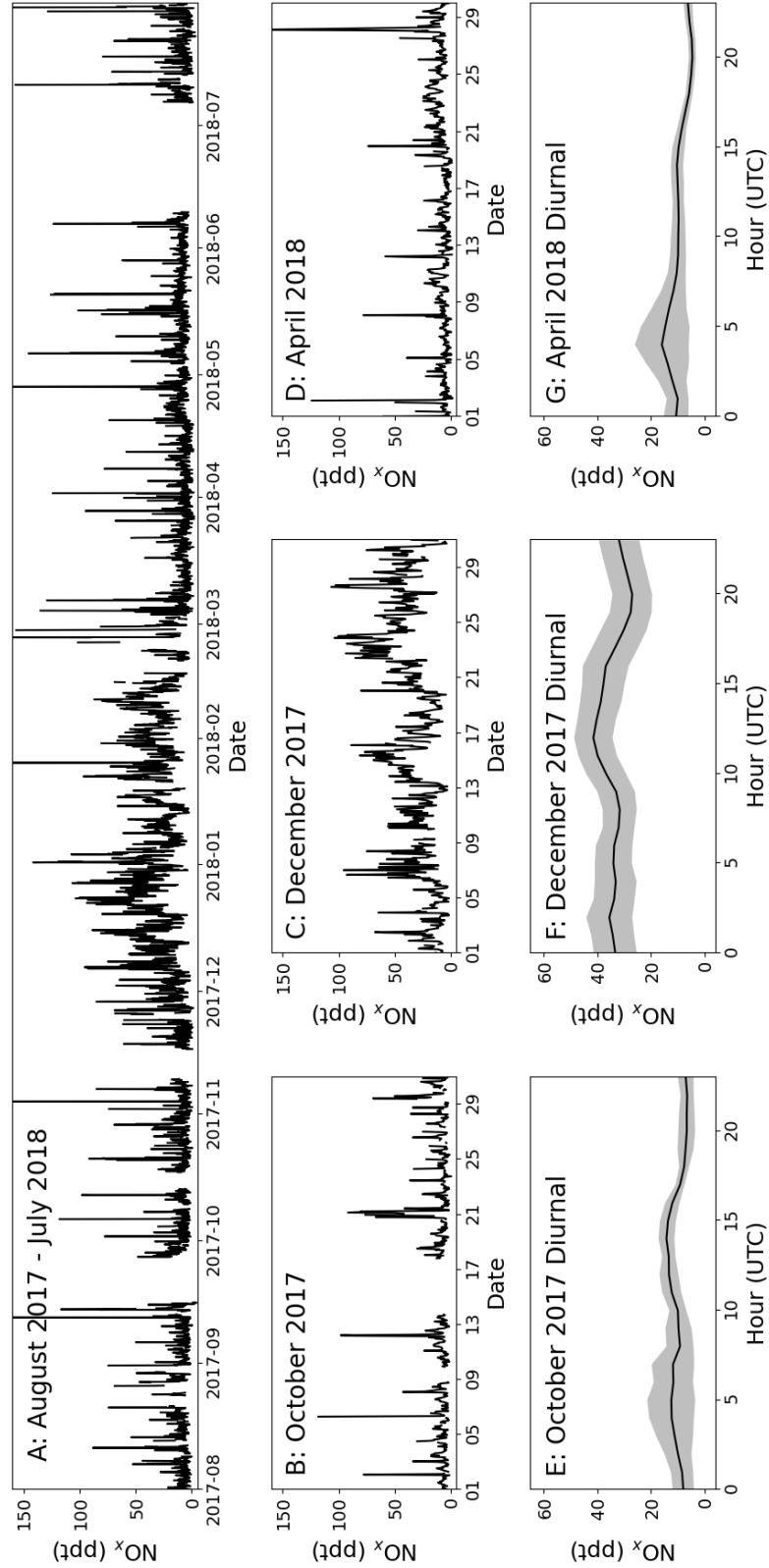
Figure 9: Panel A show the time series for total $NO_x$ (NO + $NO_2$ PLC) from August $1^{st}$ 2017 to July $31^{st}$ 2018. Panel B, C and D zoom in on October 2017, December 2017 and April 2018, respectively. Panel E, F and G show the average diurnal of $NO_x$ for October 2017, December 2017 and April 2018, respectively, with the coloured areas being $\pm 2$ standard errors. If there are less than 15 measurements available for the hour, it is not included in the diurnal.

# References

Alam, M. S., Crilley, L. R., Lee, J. D., Kramer, L. J., Pfrang, C., Vázquez-Moreno, M., Muñoz, A., Ródenas, M., and Bloss, W. J.: Interference from alkenes in chemiluminescent NOx measurements, Atmos. Meas. Tech. Discuss., 2020, 1-26, 10.5194/amt-2020-164, 2020.

Atkinson, R.: Atmospheric chemistry of VOCs and NOx, Atmospheric Environment, 34, 2063-2101, https://doi.org/10.1016/S1352-2310(99)00460-4, 2000.

Atkinson, R., Baulch, D. L., Cox, R. A., Crowley, J. N., Hampson, R. F., Hynes, R. G., Jenkin, M. E., Rossi, M. J., and Troe, J.: Evaluated kinetic and photochemical data for atmospheric chemistry: Volume I - gas phase reactions of $O_x$, $HO_x$, $NO_x$ and $SO_x$ species, Atmos. Chem. Phys., 4, 1461-1738, 10.5194/acp-4-1461-2004, 2004.

Beine, H. J., Engardt, M., Jaffe, D. A., Hov, Ø., Holme´n, K., and Stordal, F.: Measurements of NOx and aerosol particles at the NY-Å lesund Zeppelin mountain station on Svalbard: Influence of regional and local pollution sources, Atmospheric Environment, 30, 1067-1079, https://doi.org/10.1016/1352-2310(95)00410-6, 1996.

Beine, H. J., Honrath, R. E., Dominé, F., Simpson, W. R., and Fuentes, J. D.: NOx during background and ozone depletion periods at Alert: Fluxes above the snow surface, Journal of Geophysical Research: Atmospheres, 107, ACH 7-1-ACH 7-12, 10.1029/2002jd002082, 2002.

Bell, S.: A Beginner's Guide to Uncertainty of Measurement, National Physical laboratory (NPL), Teddington, Middlesex, United Kingdom, TW11 0LW,ISSN 1368-6550, 43 pp., 2001.

Berkes, F., Houben, N., Bundke, U., Franke, H., Pätz, H. W., Rohrer, F., Wahner, A., and Petzold, A.: The IAGOS NOx instrument – design, operation and first results from deployment aboard passenger aircraft, Atmos. Meas. Tech., 11, 3737-3757, 10.5194/amt-11-3737-2018, 2018.

Author: Solid-state light source photolytic nitrogen dioxide converter, US 7238328 B2, USA, USPTO, Available at: https://patents.google.com/patent/US7238328B2 (last access: 18 February 2021), 3 July 2007.

Carpenter, L. J., Fleming, Z. L., Read, K. A., Lee, J. D., Moller, S. J., Hopkins, J. R., Purvis, R. M., Lewis, A. C., Müller, K., Heinold, B., Herrmann, H., Fomba, K. W., van Pinxteren, D., Müller, C., Tegen, I., Wiedensohler, A., Müller, T., Niedermeier, N., Achterberg, E. P., Patey, M. D., Kozlova, E. A., Heimann, M., Heard, D. E., Plane, J. M. C., Mahajan, A., Oetjen, H., Ingham, T., Stone, D., Whalley, L. K., Evans, M. J., Pilling, M. J., Leigh, R. J., Monks, P. S., Karunaharan, A., Vaughan, S., Arnold, S. R., Tschritter, J., Pöhler, D., Frieß, U., Holla, R., Mendes, L. M., Lopez, H., Faria, B., Manning, A. J., and Wallace, D. W. R. J. J. o. A. C.: Seasonal characteristics of tropical marine boundary layer air measured at the Cape Verde Atmospheric Observatory, 67, 87-140, 10.1007/s10874-011-9206-1, 2010.

Carroll, M. A., Ridley, B. A., Montzka, D. D., Hubler, G., Walega, J. G., Norton, R. B., Huebert, B. J., and Grahek, F. E.: Measurements of nitric oxide and nitrogen dioxide during the Mauna Loa Observatory Photochemistry Experiment, Journal of Geophysical Research: Atmospheres, 97, 10361-10374, 10.1029/91jd02296, 1992.

Carsey, T. P., Churchill, D. D., Farmer, M. L., Fischer, C. J., Pszenny, A. A., Ross, V. B., Saltzman, E. S., Springer-Young, M., and Bonsang, B.: Nitrogen oxides and ozone production in the North Atlantic marine boundary layer, Journal of Geophysical Research: Atmospheres, 102, 10653-10665, 10.1029/96JD03511, 1997.

Carslaw, D. C.: Evidence of an increasing NO2/NOX emissions ratio from road traffic emissions, Atmospheric Environment, 39, 4793-4802, https://doi.org/10.1016/j.atmosenv.2005.06.023, 2005.

Chiapello, I., Bergametti, G., Gomes, L., Chatenet, B., Dulac, F., Pimenta, J., and Suares, E. S.: An additional low layer transport of Sahelian and Saharan dust over the north-eastern Tropical Atlantic, Geophysical Research Letters, 22, 3191-3194, 10.1029/95gl03313, 1995.

Clough, P., and Thrush, B. A.: Mechanism of chemiluminescent reaction between nitric oxide and ozone, Transactions of the Faraday Society, 63, 915-925, 1967.

Clyne, M. A. A., Thrush, B. A., and Wayne, R. P.: Kinetics of the chemiluminescent reaction between nitric oxide and ozone, Transactions of the Faraday Society, 60, 359-370, 10.1039/TF9646000359, 1964.

Drummond, J. W., Volz, A., and Ehhalt, D. H.: An optimized chemiluminescence detector for tropospheric NO measurements, Journal of Atmospheric Chemistry, 2, 287-306, 1985.

Dunlea, E. J., Herndon, S. C., Nelson, D. D., Volkamer, R. M., San Martini, F., Sheehy, P. M., Zahniser, M. S., Shorter, J. H., Wormhoudt, J. C., Lamb, B. K., Allwine, E. J., Gaffney, J. S., Marley, N. A., Grutter, M., Marquez, C., Blanco, S., Cardenas, B., Retama, A., Ramos Villegas, C. R., Kolb, C. E., Molina, L. T., and Molina, M. J.: Evaluation of nitrogen dioxide chemiluminescence monitors in a polluted urban environment, Atmos. Chem. Phys., 7, 2691-2704, 10.5194/acp-7-2691-2007, 2007.

Finlayson, B. J., Pitts, J. N., and Atkinson, R.: Low-pressure gas-phase ozone-olefin reactions. Chemiluminescence, kinetics, and mechanisms, Journal of the American Chemical Society, 96, 5356-5367, 10.1021/ja00824a009, 1974.

Fomba, K. W., Müller, K., van Pinxteren, D., Poulain, L., van Pinxteren, M., and Herrmann, H.: Long-term chemical characterization of tropical and marine aerosols at the Cape Verde Atmospheric Observatory (CVAO) from 2007 to 2011, Atmos. Chem. Phys., 14, 8883-8904, 10.5194/acp-14-8883-2014, 2014.

Fontijn, A., Sabadell, A. J., and Ronco, R. J.: Homogeneous chemiluminescent measurement of nitric oxide with ozone. Implications for continuous selective monitoring of gaseous air pollutants, Analytical chemistry, 42, 575-579, 1970.

Galbally, I. E.: Nitrogen Oxides (NO, $NO_2$, $NO_y$) measurements at Cape Grim: A technical manual CSIRO, Australia, 119 pp., 2020, https://doi.org/10.25919/dt6y-3q53.

Gilge, S., Plass-Dülmer, C., Rohrer, F., Steinbacher, M., Fjaeraa, A. M., Lagler, F., and Walden, J.: WP4-NA4: Trace gases networking: Volatile organic carbon and nitrogen oxides Deliverable D4.10: Standardized operating procedures (SOPs) for NOxy measurements, ACTRIS, 22 pp., 2014.

Grosjean, D., and Harrison, J.: Response of chemiluminescence NOx analyzers and ultraviolet ozone analyzers to organic air pollutants, Environmental Science & Technology, 19, 862-865, 10.1021/es00139a016, 1985.

Jaeglé, L., Jacob, D. J., Brune, W. H., Tan, D., Faloona, I. C., Weinheimer, A. J., Ridley, B. A., Campos, T. L., and Sachse, G. W.: Sources of HOx and production of ozone in the upper troposphere over the United States, Geophysical Research Letters, 25, 1709-1712, 10.1029/98gl00041, 1998.

Jones, A. E., Weller, R., Minikin, A., Wolff, E. W., Sturges, W. T., McIntyre, H. P., Leonard, S. R., Schrems, O., and Bauguitte, S.: Oxidized nitrogen chemistry and speciation in the Antarctic troposphere, Journal of Geophysical Research: Atmospheres, 104, 21355-21366, 10.1029/1999jd900362, 1999.

Kley, D., and McFarland, M.: Chemiluminescence detector for NO and $NO_2$, Atmos. Technol.;(United States), 12, 1980.

Lee, J. D., Moller, S. J., Read, K. A., Lewis, A. C., Mendes, L., and Carpenter, L. J.: Year-round measurements of nitrogen oxides and ozone in the tropical North Atlantic marine boundary layer, J Journal of Geophysical Research: Atmospheres, 114, 2009.

Logan, J. A.: Tropospheric ozone: Seasonal behavior, trends, and anthropogenic influence, 90, 10463-10482, doi:10.1029/JD090iD06p10463, 1985.

Matthews, R. D., Sawyer, R. F., and Schefer, R. W.: Interferences in chemiluminescent measurement of nitric oxide and nitrogen dioxide emissions from combustion systems, Environmental Science & Technology, 11, 1092-1096, 10.1021/es60135a005, 1977.

Mazzeo, N. A., Venegas, L. E., and Choren, H.: Analysis of NO, $NO_2$, $O_3$ and $NO_x$ concentrations measured at a green area of Buenos Aires City during wintertime, Atmospheric Environment, 39, 3055-3068, https://doi.org/10.1016/j.atmosenv.2005.01.029, 2005.

Monks, P. S., Carpenter, L. J., Penkett, S. A., Ayers, G. P., Gillett, R. W., Galbally, I. E., and Meyer, C. P.: Fundamental ozone photochemistry in the remote marine boundary layer: the soapex experiment, measurement and theory, Atmospheric Environment, 32, 3647-3664, https://doi.org/10.1016/S1352-2310(98)00084-3, 1998.

Pandey, S. K., Kim, K.-H., Chung, S.-Y., Cho, S. J., Kim, M. Y., and Shon, Z.-H.: Long-term study of NOx behavior at urban roadside and background locations in Seoul, Korea, Atmospheric Environment, 42, 607-622, https://doi.org/10.1016/j.atmosenv.2007.10.015, 2008.

Peterson, M. C., and Honrath, R. E.: $NO_x$ and $NO_y$ over the northwestern North Atlantic: Measurements and measurement accuracy, Journal of Geophysical Research: Atmospheres, 104, 11695-11707, 1999.

Pisso, I., Sollum, E., Grythe, H., Kristiansen, N. I., Cassiani, M., Eckhardt, S., Arnold, D., Morton, D., Thompson, R. L., Groot Zwaaftink, C. D., Evangeliou, N., Sodemann, H., Haimberger, L., Henne, S., Brunner, D., Burkhart, J. F., Fouilloux, A., Brioude, J., Philipp, A., Seibert, P., and Stohl, A.: The Lagrangian particle dispersion model FLEXPART version 10.4, Geosci. Model Dev., 12, 4955-4997, 10.5194/gmd-12-4955-2019, 2019.

Pollack, I. B., Lerner, B. M., and Ryerson, T. B.: Evaluation of ultraviolet light-emitting diodes for detection of atmospheric NO2 by photolysis - chemiluminescence, Journal of Atmospheric Chemistry, 65, 111-125, 10.1007/s10874-011-9184-3, 2010.

Read, K. A., Mahajan, A. S., Carpenter, L. J., Evans, M. J., Faria, B. V. E., Heard, D. E., Hopkins, J. R., Lee, J. D., Moller, S. J., Lewis, A. C., Mendes, L., McQuaid, J. B., Oetjen, H., Saiz-Lopez, A., Pilling, M. J., and Plane, J. M. C.: Extensive halogen-mediated ozone destruction over the tropical Atlantic Ocean, Nature, 453, 1232, 10.1038/nature07035

https://www.nature.com/articles/nature07035#supplementary-information, 2008.

Reed, C., Evans, M. J., Carlo, P. D., Lee, J. D., Carpenter, L. J. J. A. C., and Physics: Interferences in photolytic NO 2 measurements: explanation for an apparent missing oxidant?, 16, 4707-4724, 2016.

Reed, C., Evans, M. J., Crilley, L. R., Bloss, W. J., Sherwen, T., Read, K. A., Lee, J. D., and Carpenter, L. J.: Evidence for renoxification in the tropical marine boundary layer, Atmos. Chem. Phys., 17, 4081-4092, 10.5194/acp-17-4081-2017, 2017.

Rhoads, K. P., Kelley, P., Dickerson, R. R., Carsey, T. P., Farmer, M., Savoie, D. L., and Prospero, J. M.: Composition of the troposphere over the Indian Ocean during the monsoonal transition, Journal of Geophysical Research: Atmospheres, 102, 18981-18995, 10.1029/97JD01078, 1997.

Ridley, B. A., Carroll, M. A., and Gregory, G. L.: Measurements of nitric oxide in the boundary layer and free troposphere over the Pacific Ocean, Journal of Geophysical Research: Atmospheres, 92, 2025-2047, 10.1029/JD092iD02p02025, 1987.

Ridley, B. A., and Grahek, F. E.: A Small, Low Flow, High Sensitivity Reaction Vessel for NO Chemiluminescence Detectors, Journal of Atmospheric and Oceanic Technology, 7, 307-311, 10.1175/1520-0426(1990)007<0307:Aslfhs>2.0.Co;2, 1990.

Ridley, B. A., Grahek, F. E., and Walega, J. G.: A Small High-Sensitivity, Medium-Response Ozone Detector Suitable for Measurements from Light Aircraft, Journal of Atmospheric and Oceanic Technology, 9, 142-148, 10.1175/1520-0426(1992)009<0142:Ashsmr>2.0.Co;2, 1992.

Rijkenberg, M. J. A., Powell, C. F., Dall'Osto, M., Nielsdottir, M. C., Patey, M. D., Hill, P. G., Baker, A. R., Jickells, T. D., Harrison, R. M., and Achterberg, E. P.: Changes in iron speciation following a Saharan dust event in the tropical North Atlantic Ocean, Marine Chemistry, 110, 56-67, https://doi.org/10.1016/j.marchem.2008.02.006, 2008.

Ryall, D. B., Derwent, R. G., Manning, A. J., Simmonds, P., and O'Doherty, S.: Estimating source regions of European emissions of trace gases from observations at Mace Head, 2507-2523 pp., 2001.

Ryerson, T. B., Williams, E. J., and Fehsenfeld, F. C.: An efficient photolysis system for fast-response NO2 measurements, Journal of Geophysical Research: Atmospheres, 105, 26447-26461, 10.1029/2000jd900389, 2000.

Stohl, A., Hittenberger, M., and Wotawa, G.: Validation of the lagrangian particle dispersion model FLEXPART against large-scale tracer experiment data, Atmospheric Environment, 32, 4245-4264, https://doi.org/10.1016/S1352-2310(98)00184-8, 1998.

Torres, A. L., and Thompson, A. M.: Nitric oxide in the equatorial Pacific boundary layer: SAGA 3 measurements, Journal of Geophysical Research: Atmospheres, 98, 16949-16954, 10.1029/92jd01906, 1993.

Val Martin, M., Honrath, R., Owen, R. C., Pfister, G., Fialho, P., and Barata, F. J. J. o. G. R. A.: Significant enhancements of nitrogen oxides, black carbon, and ozone in the North Atlantic lower free troposphere resulting from North American boreal wildfires, 111, 2006.

Val Martin, M., Honrath, R. E., Owen, R. C., and Li, Q. B.: Seasonal variation of nitrogen oxides in the central North Atlantic lower free troposphere, Journal of Geophysical Research: Atmospheres, 113, 10.1029/2007jd009688, 2008.

Winer, A. M., Peters, J. W., Smith, J. P., and Pitts, J. N.: Response of commercial chemiluminescent nitric oxide-nitrogen dioxide analyzers to other nitrogen-containing compounds, Environmental Science & Technology, 8, 1118-1121, 10.1021/es60098a004, 1974.